Contact ageing in atomic friction

2008 J. Phys.: Condens. Matter 20 354001

(http://iopscience.iop.org/0953-8984/20/35/354001)

J. Phys.: Condens. Matter **20** (2008) 354001 (7pp) doi:10.1088/0953-8984/20/35/354001

Contact ageing in atomic friction

M Evstigneev[1], A Schirmeisen[2], L Jansen[2], H Fuchs[2] and P Reimann[1]

[1] Fakultät für Physik, Universität Bielefeld, Universitätsstraße 25, 33615 Bielefeld, Germany
[2] Center for Nanotechnology (CeNTech), Universität Münster, Heisenbergstraße 11, 48149 Münster, Germany

E-mail: Mykhaylo@Physik.Uni-Bielefeld.De

Received 28 January 2008
Published 11 August 2008
Online at stacks.iop.org/JPhysCM/20/354001

Abstract

The stick–slip motion of an atomic force microscope cantilever on highly oriented pyrolytic graphite is investigated experimentally and theoretically. It is shown that the interstitial slips of the cantilever tip at high pulling velocities are thermally activated events and can be described with a single-step rate equation. On the other hand, at slow pulling, the statistics of the slip events deviates from the predictions of the single-step rate approach, signaling the onset of contact ageing, that is, gradual changes of the contact properties in each stick phase. A model is introduced which takes the contact ageing effect into account, and whose predictions are in good agreement with the experimental results for all pulling velocities.

1. Introduction

The invention [1] and constant further development [2, 3] of atomic force microscopy (AFM) has led to tremendous progress in our abilities to experimentally characterize the properties of nanosized objects. Among the first research applications of AFM was the pioneering work by Mate *et al* [4] dedicated to friction at the nanoscale. Friction force microscopy (FFM), or the study of tribological properties of materials on such length scales, is not only important for fundamental research, but also for a number of (nano)technological applications.

In a typical FFM experiment [4], the tip of an AFM cantilever is brought into contact with a uniformly moving atomically clean surface while a normal load F_N is applied (see figure 1). The interaction between the tip and the surface leads to torsional deformations of the cantilever beam. One can determine the magnitude of these deformations by optical means and thus deduce the resulting elastic force $f_{\exp}(t)$, which, by Newton's third law, equals the instantaneous force of friction. As a rule, the temporal evolution of the friction force proceeds in a sawtooth-like pattern (see figure 2(b) below). The central quantity of interest is the behavior of the time-averaged friction force

$$\bar{f} := \lim_{t\to\infty} \frac{1}{t} \int_0^t \mathrm{d}t'\, f_{\exp}(t') \qquad (1)$$

as a function of the pulling velocity v.

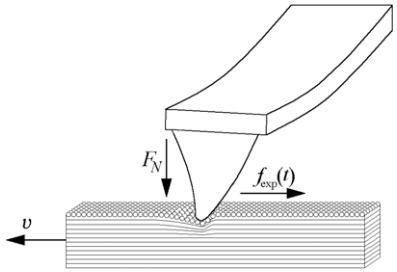

Figure 1. Schematic illustration of an FFM experiment.

It has been experimentally established [5–11] that the average force increases approximately logarithmically with velocity. This experimental finding has been interpreted using the Prandtl–Tomlinson model [12, 13] modified by inclusion of noise effects. Qualitatively, the physical picture is as follows. The motion of the cantilever tip consists of alternating stick and slip phases. During a stick phase, the tip is confined within one of the lattice sites of the surface and, in the frame of reference of the cantilever, moves together with it. This leads to an increase of the elastic deformation within the cantilever and the surface in the contact region, and, correspondingly, to the reduction of the potential barrier separating the tip from the next lattice site. At some point, the thermal noise, which is inevitably present in any physical system, drives the tip over this barrier into the new site, and the new stick phase begins.

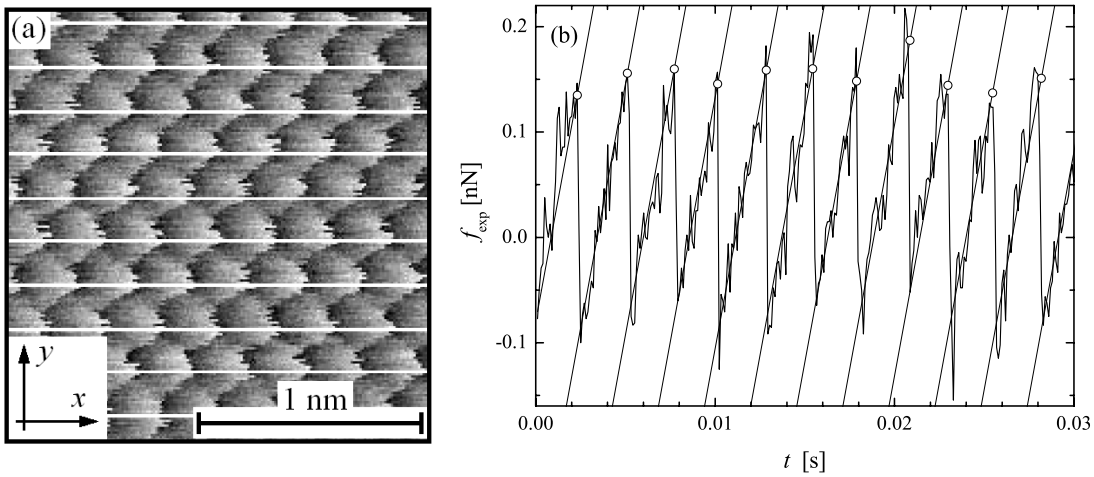

Figure 2. (a) A representative lateral force map on HOPG obtained at a pulling velocity $v = 100$ nm s^{-1}. The horizontal lines indicate the scan lines which were used for the collection of friction data. (b) The experimentally observed lateral force $f_{exp}(t)$ during one typical line scan from (a). The equidistant parallel lines result from the fit of the stick segments with (5) as detailed in the text. The circles show the positions of the slip events.

To model this process quantitatively, Kramers' theory of thermally activated transitions is often used [7, 10, 11, 14–19]. Within this approach, the probability $p(t)$ of staying within the same potential well of the tip–sample interaction potential up to time t decays according to the single-step reaction equation

$$\dot{p}(t) = -\omega(f(t))p(t), \tag{2}$$

where the exponentially disadvantaged back-transitions are neglected. The rate $\omega(f(t))$ of thermally activated jumps into the next well under the action of the elastic force $f(t)$ is given by the Kramers–Arrhenius law

$$\omega(f) = \nu_0 \exp(-\Delta E(f)/kT). \tag{3}$$

Here, the attempt frequency ν_0 depends only weakly on f, and $\Delta E(f)$ is the force-dependent height of the potential barrier, which can be approximated as

$$\Delta E(f) = \Delta E_0 (1 - f/F_0)^{\alpha} \tag{4}$$

where ΔE_0 is the force-free height of the barrier that the tip needs to surmount in order to slip into the next lattice site, F_0 is the critical force at which the barrier disappears, and the exponent α controls how fast the barrier height goes from the initial value ΔE_0 at $f = 0$ to zero at $f = F_0$. Usually, this exponent is close to 1 [8, 10, 11, 14, 15, 20]. Since the rate $\omega(f)$ determines the number of slips per unit time, the force–velocity relation has the generic form $v \propto \omega(\bar{f}_{slip})$ with $\bar{f}_{slip}$ being the average force at the moment of slip [16, 17]; taking into account (3), we find that $\bar{f}_{slip} \propto |\ln v|^{1/\alpha}$.

Although this relation between the pulling velocity and the friction force has been shown to agree well with the experimental data [11], we argue that this success does not prove unambiguously the validity of the simple rate equation (2) for the description of the stick–slip process. Indeed, apart from thermal noise effects encapsulated in (2), other sources of randomness of jump events are conceivable in experiments. Some of them are as follows.

The tip–substrate contact is a complicated system involving many atoms. After each slip, the contact is formed anew, and there is no *a priori* reason to expect that all participating atoms will establish the same positions and interactions in the new stick phase as in the previous one. Furthermore, the cantilever tip may even acquire or lose surface atoms during a stick–slip cycle. Because of the exponential form of the rate (3), even a small variation of contact properties may result in large variations of $\omega(f)$ in the rate equation (2). Finally, it has been suggested recently [21, 22] that the tip forms multiple contacts, whose behavior cannot be captured by a single-step rate equation (2), but rather requires a more complicated multiple-step model describing several possible bonds in the contact region.

Because the rate $\omega(f)$ determines the number of interstitial transitions per unit time, the logarithmic force–velocity relation reflects the exponential character of this function. Since in all cases mentioned above it is not necessary to abandon the rate description concept, but rather amend it, all of these possibilities preserve the logarithmic character of the force–velocity relation. However, when fitting the experimental force–velocity curve according to the simple rate equation (2) [7, 11], it remains unclear what exactly the resulting fitting parameters characterize—a single tip–sample contact, the average effect of differently formed contacts in each stick phase, multicontact connection between the tip and the substrate, or possibly some other mechanism not mentioned above? To resolve this ambiguity, it is imperative to *directly* check the validity of the rate equation itself (2) in each experimental situation.

In the next section, the method of data analysis originally presented in the context of dynamic force spectroscopy [23] is adapted to the present case in order to test the validity of the single-step rate equation (2) based on the statistics of the slip events and, upon confirming the validity of (2), accurately deduce the rate $\omega(f)$. Then, the details of the experiment are presented and this method of data analysis is

applied to nanofriction on highly oriented pyrolytic graphite (HOPG). It has been found in the work [24] that the rate equation (2) is experimentally valid only at relatively large pulling velocities, and this finding was interpreted as evidence for contact ageing, i.e., gradual change of contact properties with time due to formation of additional tip–substrate bonds. In the present work, we go one step further and introduce a minimalistic model, which allows one to account quantitatively for this effect, and whose predictions are in a good agreement with the experimental data for all pulling velocities probed experimentally.

2. Analysis of the experimental data

During each stick phase, the elastic force is known to increase linearly with time (see figure 2(b)),

$$f_n(t) = \kappa(vt - na) + \Delta f, \tag{5}$$

where v is the pulling velocity, a is the lattice constant, κ is the effective spring constant, describing the combined effect of the elastic deformation of the cantilever, the surface in the contact region, and the curvature of the tip–sample interaction potential [17, 25], and Δf is some additive constant. With the change of variables (5), we find from the rate equation (2) that the no-jump probability $p_v(f)$ up to the force f at a pulling velocity v decays as $\kappa v\, \mathrm{d}p_v(f)/\mathrm{d}f = -\omega(f)\, p_v(f)$, where we have dropped the redundant index n, as this no-jump probability in the force domain is the same for all stick phases. Given the initial condition that the tip was in a given potential well at the force value f_0 (i.e. $p(f_0) = 1$), the solution of this equation reads

$$p_v(f) = \exp\left(-\frac{1}{\kappa v}\int_{f_0}^{f} \mathrm{d}f'\omega(f')\right). \tag{6}$$

Given the number $N_v(f)$ of stick phases which ended at force values greater than f at velocity v, the best experimental estimate for the probability of staying within the same well up to the force f is given by

$$\tilde{p}_v(f) = N_v(f)/N_v(f_0). \tag{7}$$

Here and in the following, a tilde indicates an experimental estimate for the corresponding 'true' quantity without a tilde, towards which it converges (with probability 1) for $N_v(f_0) \to \infty$.

We now come to the central point of this section, namely the simple observation that, according to (6), the function

$$g_v(f) := -\kappa v \ln p_v(f) = \int_{f_0}^{f} \mathrm{d}f'\omega(f') \tag{8}$$

is in fact independent of the pulling speed v. The convergence of the experimental estimate

$$\tilde{g}_v(f) = -\kappa v \ln \tilde{p}_v(f) = -\kappa v \ln[N_v(f)/N_v(f_0)] \tag{9}$$

to its true value (8) is not uniform, because for any pulling velocity v, the majority of slip events occur in a rather limited force interval around the most probable slip force, which logarithmically increases with pulling velocity. However, by properly exploiting the velocity independence of the g-function, it is possible to reliably estimate $g(f)$ over a wide f-range by combining data for several different pulling speeds v.

Consider an arbitrary but fixed $f > f_0$. Then, the reliability of the estimate (9) is quantified by the variance $\tilde{\sigma}^2[\tilde{g}_v(f)]$, whose explicit determination will be given shortly. With this amount of information at our disposal, according to the so called method of weighted averages [26], the best guess for the 'true' $g(f)$ is represented by that argument x which minimizes the weighted sum of square deviations $\sum_v [x - \tilde{g}_v(f)]^2/\tilde{\sigma}^2[\tilde{g}_v(f)]$, where $\sum_v$ indicates a summation over all pulling velocities v probed experimentally [23]. In other words, this best guess for $g(f)$ is given by the weighted average

$$\tilde{g}(f) = \sum_v c_v(f)\, \tilde{g}_v(f), \tag{10}$$

$$c_v(f) := \frac{1}{\tilde{\sigma}^2[\tilde{g}_v(f)]} \Big/ \sum_v \frac{1}{\tilde{\sigma}^2[\tilde{g}_v(f)]}. \tag{11}$$

In order to determine the variances $\tilde{\sigma}^2[\tilde{g}_v(f)]$, we consider the number $N_v(f) = p_v(f)\, N_v(f_0)$ of stick phases surviving up to the pulling force f. It follows that for any fixed f, v, and $N_v(f_0)$, the number $N_v(f)$ is distributed binomially according to

$$W(N_v(f)) = \frac{[p_v(f)]^{N_v(f)}[1 - p_v(f)]^{N_v(f_0)-N_v(f)} N_v(f_0)!}{N_v(f)![N_v(f_0) - N_v(f)]!}, \tag{12}$$

implying for the associated variance $\sigma^2[N_v(f)]$ the result

$$\sigma^2[N_v(f)] = N_v(f_0)\, p_v(f)[1 - p_v(f)]. \tag{13}$$

An estimate $\tilde{\sigma}^2[N_v(f)]$ for the 'true' $\sigma^2[N_v(f)]$ follows on replacing the 'true' but unknown $p_v(f)$ in (13) by the estimate $\exp[-\tilde{g}(f)/(\kappa v)]$ (see (6), (8)). Then, by exploiting the error propagation law $\tilde{\sigma}^2[\tilde{g}_v(f)] = [\mathrm{d}\tilde{g}_v(f)/\mathrm{d}N_v(f)]^2\, \tilde{\sigma}^2[N_v(f)]$ and (9), one finds for the coefficients c_v in (11) the result

$$c_v(f) = \frac{N_v(f_0)\, \tilde{p}_v^2(f)\, \mathrm{e}^{\tilde{g}(f)/v}}{v^2\,[1 - \mathrm{e}^{-\tilde{g}(f)/v}]}\, \sigma^2[\tilde{g}(f)] \tag{14}$$

$$\sigma^2[\tilde{g}(f)] := \left(\sum_v \frac{N_v(f_0)\, \tilde{p}_v^2(f)\, \mathrm{e}^{\tilde{g}(f)/v}}{v^2\,[1 - \mathrm{e}^{-\tilde{g}(f)/v}]}\right)^{-1}. \tag{15}$$

Finally, by taking into account (11) one readily verifies that $\sigma^2[\tilde{g}(f)]$ from (15) does indeed coincide with the variance $\sum_v c_v^2\, \tilde{\sigma}^2[\tilde{g}_v(f)]$ describing the statistical uncertainty of $\tilde{g}(f)$ in (10).

In practice, the above method reduces to the following two steps. First, the functions $\tilde{p}_v(f)$ and $\tilde{g}_v(f)$ are determined from the experimentally observed rupture forces f_n, $n = 1, \ldots, N_v(f_0)$, for different pulling speeds v according to (7) and (9). Second, the weighted average (10), (14) is evaluated. Since the coefficients $c_v(f)$ in (10) depend themselves on the unknown quantity $\tilde{g}(f)$ according to (14), we are dealing with a transcendental equation for $\tilde{g}(f)$ for any fixed f-value. Among many other well-known methods for solving such an

equation, one particularly simple way is to iteratively update the value of $\tilde{g}(f)$ on the basis of (10) until stationarity is reached. The result is an estimate $\tilde{g}(f)$ for the 'true' function $g(f)$ in (8) together with its statistical uncertainty (15). Once a specific f-dependence of the rate $\omega(f)$, as e.g. in (3), (4), is assumed, it is possible to decide using (8) whether this assumption is compatible with the measured data and to determine the fit parameters. In addition, one can check whether the functions $\tilde{g}_v(f)$ for different pulling velocities v do indeed collapse within their statistical uncertainties onto a single master curve. If this is not the case, it follows that the basic kinetic law (2) does not describe the experimental stick–slip data adequately.

3. Experiment

The friction force experiments were conducted with a commercial AFM (Omicron VT-AFM) under the pressure of 2×10^{-10} mbar at room temperature. The sample was highly oriented pyrolytic graphite (HOPG) cleaved in the load lock in vacuum at $p = 10^{-9}$ mbar shortly before the AFM experiments. As force sensors, we used single-crystalline rectangular silicon cantilevers (LFMR type, from Nanosensors) of width 43 μm, length 229 μm and tip height 15 μm. Their thickness was determined from the resonance frequency of the normal oscillations in vacuum [27]. The normal and torsional spring constants of the cantilever were calculated from the geometric dimensions [28] yielding 0.18 N m^{-1} and 19.0 N m^{-1}, respectively (with the E-modulus 169 GPa and shear modulus 50 GPa). We calibrated the lateral force sensitivity of the AFM using a procedure analogous to the one described in [18, 29]. The tip–sample adhesion force was determined from the average jump-off-contact value $F_{\mathrm{off}} = 11.2$ nN. Since an additional load of $F_{\mathrm{load}} = 33.4$ nN was applied, the effective load during the friction experiments was $F_{\mathrm{off}} + F_{\mathrm{load}} = 44.6$ nN.

Larger areas (1 μm $\times$ 1 μm) of the HOPG sample were first scanned in order to verify that a flat and homogeneous part of the surface with no steps was investigated. Smaller scan areas of 3 nm $\times$ 3 nm were used to identify atomic jump processes; see figure 2(a). The stick–slip phenomenon is observed via the friction force contrast with atomic unit-cell periodicity of the surface. A typical friction signal for a single scan line is shown in figure 2(b) revealing the expected sawtooth-type behavior. The velocity dependence of the friction forces was measured in the range from $v = 20$ to 200 nm s^{-1}.

The individual carbon atoms form hexagonal rings arranged in a honeycomb structure [30]. During the scan, the tip jumps in between the local energy minima located at the centers of the carbon rings ('hollow sites' [30] appearing as 'humps' in figure 2(a)). We oriented the sample in such a way that the fast scan direction (x-direction) scans along the $(\bar{1}, 2, \bar{1}, 0)$ direction of the (0001) HOPG surface. This ensures that predominantly jumps along the fast scan direction are observed [18]. Since the surface potential varies along the y-axis even within one hollow site, we use for our analysis only the scan lines from the equivalent y-positions at the centers of the hollow sites. Those positions are indicated with the horizontal lines in figure 2(a).

4. Results

A typical stick–slip scan line contained 10–12 slip events; see figure 2(b). While the moments t_n of the slip events can be readily identified as almost instantaneous force drops, the forces themselves require a more careful consideration. As seen in figure 2(b), the experimentally observed force evolution $f_{\mathrm{exp}}(t)$ is composed of random fluctuations due to thermal and instrumental noise, whose details strongly depend on the experimental set-up, and linearly increasing regular segments, which represent the force f entering the theory (2)–(8). Hence, the random forces have to be separated from the regular ones in the experimental data before comparison with the theory. To this end, we fitted the measured $f_{\mathrm{exp}}(t)$ in figure 2(b) with a piecewise linear function of the form (5), increasing its index n at every previously determined slip instant t_n. As a result, each scan line yields an estimate for the unknown fit parameters in (5), namely the effective spring constant κ and the lattice constant a. Moreover, evaluating the fitting function at the slip times t_n yields the force values at the end of every stick phase, indicated by the circles in figure 2(b), and required to evaluate the theoretical quantities in (6), (8) and also in (23) below.

By fitting a and κ for each scan line, the former was found to vary only insignificantly around the mean value $a \simeq 0.26$ nm, while the latter fluctuated by about 8% (standard deviation) around the mean value $\kappa \simeq 0.93$ N m^{-1}. These variations can be understood as a signature of the complicated behavior of the tip–substrate contact, considering that the tip apex is particularly prone to changes at the very beginning of every scan line and that the tip–substrate contact significantly influences the relevant effective spring constant κ [25, 31].

As outlined above, our main goal is to check by means of (8) whether the individual slip events can be viewed as single-step transitions (2). Note that the force dependence of the rate $\omega(f)$ in (3) is quite sensitive to changes of the effective spring constant κ, and in (8) it is tacitly assumed that only one fixed value of κ exists. Due to the above-mentioned variability of κ we thus cannot use all available stick–slip data, but rather have to restrict ourselves to a subset for which κ is confined to a narrow window around some specific value. We have processed data sets for several such values of κ and found practically the same results for all of them. In the following, we report our findings for $0.92 \text{ N m}^{-1} \leqslant \kappa \leqslant 0.94 \text{ N m}^{-1}$.

As shown in figure 3(a), the measured functions $\tilde{g}_v(f)$ do indeed collapse onto a single master curve, provided that the pulling velocities are sufficiently high, $v > 90$ nm s^{-1}. On the other hand, no such collapse is observed in the low-velocity range (see figure 3(b)), where the experimental g-function increases with increasing pulling velocity. This result indicates the inapplicability of the rate theory (2) to the description of the stick–slip process at slow pulling. In the following section we amend the model (2) to adequately describe the experimental results for all pulling velocities.

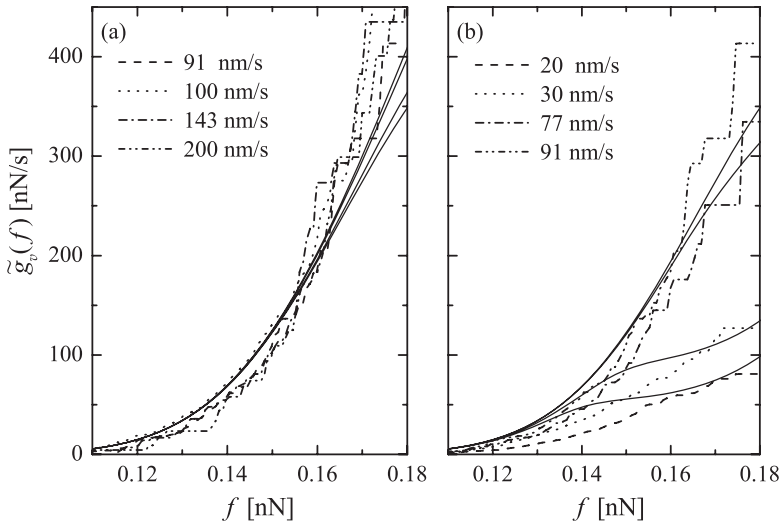

Figure 3. The experimentally measured functions $\tilde{g}_v(f)$ from (9) for different pulling velocities, v, as specified in the legends, for zero initial force, $f_0 = 0$, and for the effective spring constants $0.92\ \mathrm{N\ m^{-1}} \leqslant \kappa \leqslant 0.94\ \mathrm{N\ m^{-1}}$. The smooth solid lines are theoretical fits, using the model described in section 5.

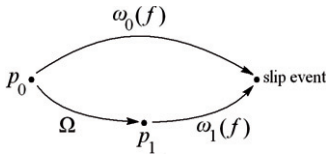

Figure 4. Schematic representation of the proposed model of the tip–sample contact.

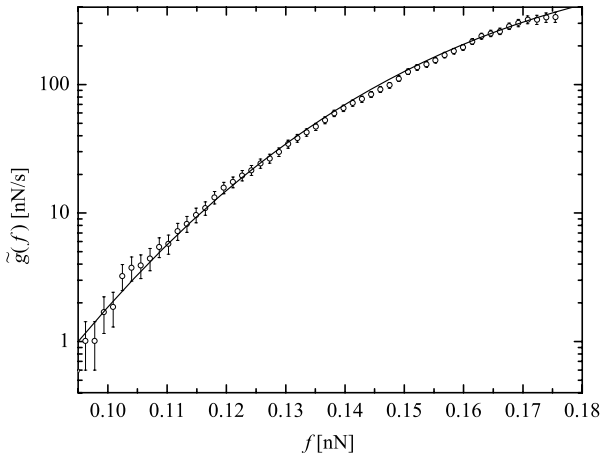

Figure 5. Circles: the combined function $\tilde{g}(f)$ based on the experimental g-curves for $90\ \mathrm{nm\ s^{-1}} < v \leqslant 200\ \mathrm{nm\ s^{-1}}$. Solid line: theoretical fit using (23).

5. Modeling

The lack of universal behavior of the g-function for slow velocities (figure 3(b)) indicates the inapplicability of the single-step rate description (2) and suggests that some other process besides thermal activation plays a significant role in this regime, while at fast pulling, thermal activation takes over. In the spirit of [21, 22], it has been hypothesized [24] that a possible candidate for such a process is multiple-bond formation for the tip–substrate contact. More precisely, formation of additional bonds takes finite time, so that at fast pulling, new bonds do not have sufficient time to develop during a single stick phase. This leaves in effect a single tip–substrate contact, whose rupture is well described by the rate equation (2), resulting in the collapse of the measured functions $\tilde{g}_v(f)$ onto a single master curve, figure 3(a).

To quantify these ideas, we introduce the following minimalistic model. We assume that, in a given stick phase, the tip–sample contact may either break, resulting in a slip event, or strengthen itself by means of forming new bonds; the latter possibility can be termed 'contact ageing'.

To account for this effect, we assume for simplicity that the contact can exist in only two different states, a strongly and a weakly bound one, characterized by two different off-rates $\omega_i(f)$, and the respective occupation probabilities $p_i(f)$, $i = 0, 1$. Here, the value of the subscript $i = 0$ refers to the initial weakly bound state of the contact, and $i = 1$ to the strongly bound state. We further assume that the contact can enter the strongly bound state 1 from the originally formed weakly bound state 0 at a rate Ω independent of the value of the force. At the same time, the back-transitions $1 \to 0$ are neglected. Our model is schematically illustrated in figure 4.

Within our simplified model, the single-step rate equation (2) describing the state of the contact should be replaced by two rate equations for the probabilities p_0, p_1:

$$\begin{aligned} \dot{p}_0(t) &= -\left[\Omega + \omega_0\big(f(t)\big)\right] p_0(t), \\ \dot{p}_1(t) &= \Omega p_0(t) - \omega_1\big(f(t)\big)\, p_1(t) \end{aligned} \tag{16}$$

with the initial condition

$$p_i(0) = \delta_{i0}. \tag{17}$$

In each stick phase, the force increases linearly (cf (5)):

$$f(t) = \kappa v t + f_0, \tag{18}$$

allowing one to go from the time to the force domain:

$$p_0'(f) = -\frac{1}{\kappa v}\left[\Omega + \omega_0(f)\right] p_0(f),$$
$$p_1'(f) = \frac{1}{\kappa v}\left[\Omega p_0(f) - \omega_1(f) p_1(f)\right]. \tag{19}$$

From these equations, one obtains for the respective probabilities for finding the contact in the states 0 and 1 at the force f the explicit analytical results

$$p_0(f) = \exp\left[-\frac{1}{\kappa v}\left(\Omega(f - f_0) + \int_{f_0}^{f} \mathrm{d}f'\omega_0(f')\right)\right],$$
$$p_1(f) = \frac{\Omega}{\kappa v}\int_{f_0}^{f} \mathrm{d}f' p_0(f') \exp\left(-\frac{1}{\kappa v}\int_{f'}^{f} \mathrm{d}f''\omega_1(f'')\right). \tag{20}$$

The off-rates for the two states are assumed to be given by (cf (3), (4))

$$\omega_i(f) = \nu_i \exp\left[-\frac{\Delta E_i}{k_\mathrm{B}T}\left(1 - \frac{f}{F_i}\right)^{\alpha_i}\right], \qquad i = 0, 1. \tag{21}$$

Since the probability of finding the tip in any bound state 0 or 1 is $p_0 + p_1$, the experimental g-function (9) should be compared not with the single-step result (8), but with

$$g_v(f) = -\kappa v \ln\left[p_0(f) + p_1(f)\right]. \tag{22}$$

In the limit of pulling velocities so high that new bonds do not have time to form in each stick phase, the tip remains in the state 0 throughout the whole stick phase with overwhelming probability, so the theoretical g-function (22) simplifies to a velocity-independent expression similar to (8):

$$g_\infty(f) = -\kappa v \ln p_0(f) = \int_{f_0}^{f} \mathrm{d}f'\omega_0(f')$$
$$= \frac{\nu_0 F_0}{\alpha_0}\left(\frac{k_\mathrm{B}T}{\Delta E_0}\right)^{1/\alpha_0}\left\{\gamma\left(\frac{1}{\alpha_0}, \frac{\Delta E_0}{k_\mathrm{B}T}\left(1 - \frac{f_0}{F_0}\right)^{\alpha_0}\right)\right.$$
$$\left. - \gamma\left(\frac{1}{\alpha_0}, \frac{\Delta E_0}{k_\mathrm{B}T}\left(1 - \frac{f}{F_0}\right)^{\alpha_0}\right)\right\}, \tag{23}$$

where in the second line, the integral is evaluated explicitly for the rate ansatz (21). Here, $\gamma(a, x) := \int_0^x \mathrm{d}y \mathrm{e}^{-y} y^{a-1}$ is the incomplete gamma function; it can be calculated numerically using an efficient algorithm, e.g., that from [32].

6. Fitting procedure

The theory from the previous section contains nine fit parameters, eight characterizing the rates $\omega_{0,1}(f)$ (namely, ν_i, ΔE_i, F_i, and α_i, with $i = 0, 1$), and the $0 \to 1$ transition rate Ω. Their determination proceeds consecutively in the following steps.

First, using (10), (14), (15), we have combined the g-curves in the high-velocity range (figure 3(a)) into a single master curve using the method of weighted averages, which also allows one to calculate the statistical uncertainty of the combined g-function. The plot of the g-function together with the error bars is presented in figure 5. The combined g-function from figure 5 is fitted using the high-velocity asymptotic formula (23) with the following values of the resulting fit parameters:

$$\Delta E_0 = 24\, k_\mathrm{B}T = 97.2 \text{ pN nm};$$
$$F_0 = 0.19 \text{ nN};$$
$$\alpha_0 = 2.4;$$
$$\nu_0 = 12\,000 \text{ s}^{-1}. \tag{24}$$

The fitting curve is presented in figure 5 as a solid line. The discrepancy between these values and the ones reported in [24] can be attributed to the fact that in the work [24], it was not the g-function that was fitted, but rather the rate $\omega(f)$, which was obtained by means of numerical differentiation of the experimental $\tilde{g}(f)$. Since this derivative was evaluated numerically using a finite-difference scheme, the rate fit contained an additional source of error in the resulting fit parameters.

We observe that our exponent α_0 differs significantly from the often assumed value 3/2. This can be explained as follows. The exponent α in the Kramers rate (3), (4) is directly related to the shape of the potential energy landscape of the tip as a function of its position. Approximating it with a cubic polynomial [14, 15] leads to the value $\alpha = 3/2$; on the other hand, quadratic approximation [34] leads to the value $\alpha = 2$. Our results (24) suggest that the quadratic approximation represents the tip potential more accurately than the cubic polynomial.

It remains to determine five theoretical values, namely, Ω, ν_1, ΔE_1, F_1, and α_1. To reduce their number, we make the following additional assumptions: (i) we assume that the overall geometry of the tip energy landscape in contact with the surface is the same in both states; (ii) the critical force is directly proportional to the barrier height with the same proportionality coefficient for each state; (iii) as within the Kramers theory of thermally activated escape [19], we assume that the prefactor ν_i is proportional to the value $\sqrt{U''_\mathrm{min}|U''_\mathrm{max}|}$, where U''_min and U''_max denote the curvatures of the tip energy landscape at the two extrema. These three assumptions can be expressed mathematically as

$$\alpha_1 = \alpha_0;$$
$$F_1 = \frac{\Delta E_1}{\Delta E_0} F_0;$$
$$\nu_1 = \frac{\Delta E_1}{\Delta E_0}\nu_0, \tag{25}$$

leaving only two unknown fit parameters, ΔE_1 and Ω. Their values are determined from the $\tilde{g}_v(f)$-curves in the low-velocity range (figure 3):

$$\Delta E_1 = 32\, k_\mathrm{B}T = 129.6 \text{ pN nm};$$
$$\Omega = 10 \text{ s}^{-1}. \tag{26}$$

The reasonable agreement of the fitting curves (20)–(22) with the parameters (24)–(26) with the experimental results at low velocities is clear from figure 3. From the second equation (26)

we conclude that the typical time for the formation of new bonds is of the order of $1/\Omega = 100$ ms. This number can be compared with the duration of the stick phase $\tau_{\text{stick}} = a/v \simeq 3$ ms at the slowest pulling velocity $v = 91$ nm s^{-1}, for which the validity of the rate equation (2) has been verified; see figure 3(a).

7. Concluding remarks

Although the theoretical and experimental g-curves in figure 3 are in reasonable agreement with each other, the discrepancy between the two sets of data is quite noticeable. This is because the theory presented in section 5 together with the simplifying assumptions (25) provides only a crude description of the contact ageing process, and captures only its most salient feature: changing of the contact properties in time. This crude description can be refined in several ways.

While our model uses only two contact states of the cantilever (see figure 4), one can generalize this approach and introduce additional contact states, all characterized by different occupation probabilities $p_i(f)$ and off-rates $\omega_i(f)$. In addition, the rate parameters for each such state can be considered as random variables, with respect to which the final no-jump probability $\sum_i p_i(f)$ has to be averaged [33].

Unfortunately, these amendments to the model (16) will most likely make it impossible to solve the resulting rate equations analytically, while within our simplified description, such an analytic solution is still possible; see (20)–(22). Even worse, making the above-mentioned amendments to the model (16) means introducing a number of new fit parameters, whose reasonably accurate determination based on the experimental data may be questionable.

Despite its crude simplifications, our analysis shows clearly that contact ageing plays an important role in realistic friction force experiments. The simple model presented, which can still be solved analytically, captures the essential features of this process.

Acknowledgments

The authors are grateful to the Deutsche Forschungsgemeinschaft (SFB 613, RE 1344/3-1, RE 1344/4-1, and SCHI 619/6-1) and to the ESF programs NATRIBO and FANAS (collaborative research project Nanorama—07-FANAS-FP-009) for financial support of this work.

References

[1] Binnig G, Quate C F and Gerber C 1986 *Phys. Rev. Lett.* **56** 930
[2] Meyer G and Amer N M 1988 *Appl. Phys. Lett.* **53** 1045
[3] Alexander S, Hellemans L, Marti O, Schneir J, Elings V, Hansma P K, Longmire M and Gurley J 1989 *J. Appl. Phys.* **65** 164
[4] Mate V M, McClelland G M, Erlandsson R and Chiang S 1987 *Phys. Rev. Lett.* **59** 1942
[5] Heslot F, Baumberger T, Perrin B, Caroli B and Caroli C 1994 *Phys. Rev.* E **49** 4973
[6] Bouhacina T, Aimé J P, Gauthier S, Michel D and Heroguez V 1997 *Phys. Rev.* B **56** 7694
[7] Gnecco E, Bennewitz R, Gyalog T, Loppacher Ch, Bammerlin M, Meyer E and Güntherodt H-J 2000 *Phys. Rev. Lett.* **84** 1172
[8] Sills S and Overney M 2003 *Phys. Rev. Lett.* **91** 095501
[9] Bennewitz R, Gyalog T, Guggisberg M, Bammerlin M, Meyer E and Güntherodt H-J 1999 *Phys. Rev.* B **60** R11301
[10] Gnecco E, Bennewitz R, Gyalog T and Meyer E 2001 *J. Phys.: Condens. Matter* **13** R619
[11] Riedo E, Gnecco E, Bennewitz R, Meyer E and Brune H 2003 *Phys. Rev. Lett.* **91** 084502
[12] Prandtl L 1928 *Z. Angew. Math. Mech.* **8** 85
[13] Tomlinson G A 1929 *Phil. Mag.* **7** 905
[14] Sang Y, Dubé M and Grant M 2001 *Phys. Rev. Lett.* **87** 174301
[15] Dudko O K, Filippov A E, Klafter J and Urbakh M 2002 *Chem. Phys. Lett.* **352** 499
[16] Evstigneev M and Reimann P 2005 *Phys. Rev.* E **71** 056119
[17] Evstigneev M and Reimann P 2006 *Phys. Rev.* B **73** 113401
[18] Schirmeisen A, Jansen L and Fuchs H 2005 *Phys. Rev.* B **71** 245403
[19] Hänggi P, Talkner P and Borkovec M 1990 *Rev. Mod. Phys.* **62** 251
[20] Dudko O K, Hummer G and Szabo A 2006 *Phys. Rev. Lett.* **96** 108101
[21] Filippov A E, Klafter J and Urbakh M 2004 *Phys. Rev. Lett.* **92** 135503
[22] Maier S, Sang Y, Filleter T, Grant M, Bennewitz R, Gnecco E and Meyer E 2005 *Phys. Rev.* B **72** 245418
[23] Evstigneev M and Reimann P 2003 *Phys. Rev.* E **68** R045103
[24] Evstigneev M, Schirmeisen A, Jansen L, Fuchs H and Reimann P 2006 *Phys. Rev. Lett.* **97** 240601
[25] Socoliuc A, Bennewitz R, Gnecco E and Meyer E 2004 *Phys. Rev. Lett.* **92** 134301
[26] Taylor J R 1982 *An Introduction to Error Analysis* (California: University Science Books)
[27] Sader J E, Larson I, Mulvaney P and White L R 1995 *Rev. Sci. Instrum.* **66** 3789
[28] Marti O 1990 *Handbook of Micro/Nano Tribology* ed B Bhushan (Boca Raton, FL: CRC Press)
[29] Bilas P, Romana L, Kraus B, Bercion Y and Mansot J L 2004 *Rev. Sci. Instrum.* **75** 415
[30] Hölscher H, Schwarz U D, Zwörner O and Wiesendanger R 1998 *Phys. Rev.* B **57** 2477
[31] Reimann P and Evstigneev M 2005 *New J. Phys.* **7** 25
[32] Press W H, Teukolsky S A, Vetterling W T and Flannery B P 1999 *Numerical Recipes in C* (Cambridge: Cambridge University Press)
[33] Raible M, Evstigneev M, Bartels F W, Eckel R, Nguyen-Dong M, Merkel R, Ros R, Anselmetti D and Reimann P 2006 *Biophys. J.* **90** 3851
[34] Hummer G and Szabo A 2003 *Biophys. J.* **85** 5